PROCEEDINGS, Twenty-Fourth Workshop on Geothermal Reservoir Engineering
Stanford University, Stanford, California, January 25-27, 1999
SGP-TR-162

Seismic Velocity Analysis in the Olkaria Geothermal Field

Silas Masinde Simiyu,

Geothermal Project
The Kenya Electricity Generating Company
P.O Box 785 Naivasha. Kenya

Corresponding Address: Division of Earth and Ocean Sciences
Duke University, P.O Box 90235,
Durham, NC 27708-0235

ABSTRACT

4352 local events originating within the study area [t_s-t_p<3 sec], 162 earthquakes at regional distances [5 sec<t_s-t_p<40 sec], 60 blasts from a nearby road construction quarry and 15 calibration shots are used to analyze for the hypocenter distribution and velocity variations.

The hypocenter intensity show that the brittle-ductile transition zone is at a depth of 4-5 km. V_p/V_s ratios varies from 1.58 within the East Production Field to 1.82 in the Olkaria Central Field. Poisson's ratios follow the same trend and vary from 0.15 to 0.30. The variation of σ and V_p/V_s ratio is consistent with measured reservoir fluid chemistry, pressure and temperature thus suggesting seismic parameters can be associated with reservoir properties. The low σ and V_p/V_s values are interpreted to be due to high temperature and steam/gas saturation. The result shows that measurement of σ and V_p/V_s changes in a geothermal field are useful indicators and tools for monitoring natural or induced reservoir phase changes.

INTRODUCTION

The study area is located in the Kenya rift south west of the Lake Naivasha. In this area, extensive igneous activity has occurred in the recent past and is discussed by Clarke and Woodhall (1987), Muchemi (1994), and Mungania (1995). Detailed regional and local geology with structural analysis is discussed by Muchemi [1998].

The area is comprised of geothermal fields [Figure 1] that include the Domes that is at an advanced stage of exploration and Olkaria that is under exploitation.

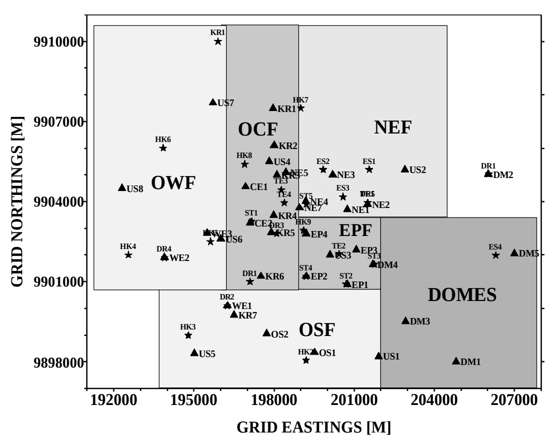

Fig. 1 Map showing the division of the study area into fields. labelled as OSF, OWF, OCF, EPF, NEF and Domes. Also Shotpoints are shown as stars and record stations astriangles.

The Olkaria Field has been divided into 5 regions based on the geology and structure [See Muna, 1998]. These are; the East

Production field [EPF] with an installed power plant currently producing 45 Mwe, the North east field [NEF] with 24 wells drilled and tested with a production capacity of 64 Mwe, the Olkaria West [OWF] field with 16 drilled wells and planned for another 64 Mwe, Olkaria Central field [OCF], and Olkaria south field [OSF].

A seismic network established in the southern Lake Naivasha area has a number of objectives that include the determination of; [I] the variation of physical parameters such as velocity of P and S waves, [ii] the event depth variations, and [iii] the effect of natural and induced phase changes within the reservoir on the $\mathbf{V_p/V_s}$ and **s**. This paper looks at the results of the analysis of these parameters.

BRITTLE-DUCTILE TRANSITION

It is well known that there is a linear increase in crustal strength with pressure [depth] and an exponential decrease in strength with temperature. Peak strength is expected at a transition point from the brittle [pressure controlled] zone called the seismogenic zone to the ductile [temperature controlled] zone [*Kohlstedt et al., 1995*]. The maximum depth in a region at which earthquakes occur in the crust will delineate the brittle-ductile transition zone [*Meissner and Strehlau, 1982*].

Fig. 2 is a depth-frequency plot for the study area and shows a change in seismic intensity at a depth of 4-5 km that might represent the brittle-ductile transition zone. This depth is reasonable given the high heat flow values [about 200 MWm^{-2}] and geothermal gradient with temperatures of more than 300^o C measured in wells at a depth of 2 km *[Wheildon et al., 1994 and Ofwona, 1998]*.

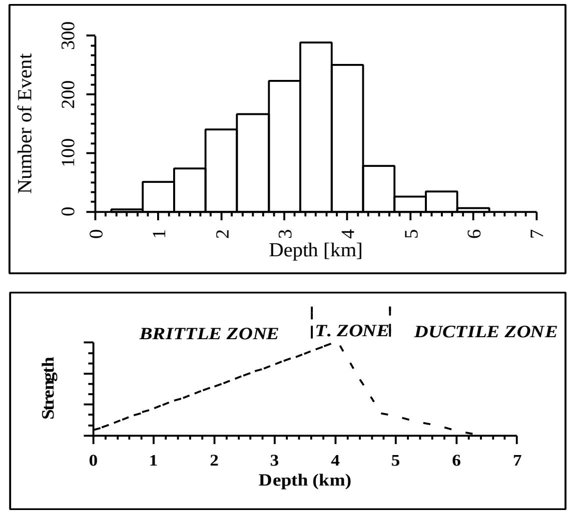

Fig 2. Plot of seismic frequency with depth and the interpreted brittle-ductile transition zone.

This depth is very important for determining the depth to the heat source, which is expected to be at 6 km. Outside the network, earthquakes deepen to the Northwest, north and north east away from the volcanic field centre.

VELOCITY ANALYSIS

V_p/V_s and Poisson's Ratio

$\mathbf{V_p/V_s}$ ratios are sensitive to phase changes in geothermal systems. Water and steam filled pore spaces affect both P and S wave transmission differently. $\mathbf{V_p/V_s}$ ratios normally increase from vapor saturated [low pore pressure] condition to liquid saturated [high pore pressure] condition [Ito et al., 1979].

Plots of P and S wave travel time versus distance for the same data set were constructed and the average velocities for P and S waves obtained by linear least-squares fit. The determined V_p was then divided by V_s to obtain the ratio. First, an average overall V_p/V_s ratio for the whole of the study area was determined and used in Hypo71 event location and then the spatial variation of the measured V_p/V_s ratio throughout the study area was determined using evenly distributed events.

V_p/V_s distribution was determined for the whole study area and found to vary from 1.55 to 1.87 with an average of 1.71. The data was then divided into smaller hypocenter-station groups consisting of earthquakes originating from one part of the field [belonging to the same swarm]. The results of the divided fields had the scatter greatly reduced and showed differing values as seen in figure 3 for the EPF, NEF, OWF, Domes, OCF and OSF

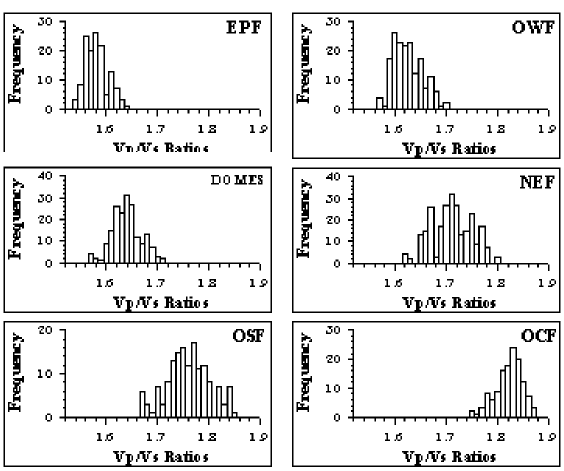

Fig. 3. Histograms of Vp/Vs variations

Fig. 4 show a map of V_p/V_s ratio contoured at 0.05 interval. Poisson's ratio **s** was estimated for a number of seismic stations using multiple earthquakes as well as at a number of epicenters using multiple seismic station data. The technique used is the construction of Wadati diagrams using the observed P and S-wave arrival times. The results showed that within the study area **s** follows closely the V_p/V_s ratios.

Average **s** for the EPF, OWF, Domes, NEF, OSF and OCF was found to be 0.16, 0.19, 0.2, 0.24, 0.26 and 0.28 respectively.

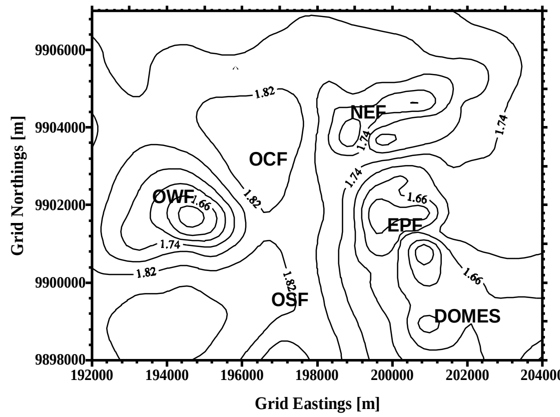

Fig. 4. Contour map of Vp/Vs variations at 0.05 interval

RESERVOIR CONSIDERATION

North East Field [NEF]

The Northeast field is at an advanced stage of development and has 24 wells that have been tested for a 64 Mwe power station. Detailed analysis of V_p/V_s ratio for the NEF [Fig. 5] show that the central area it's characterized by low values consistent with the presence of a steam zone and higher temperatures

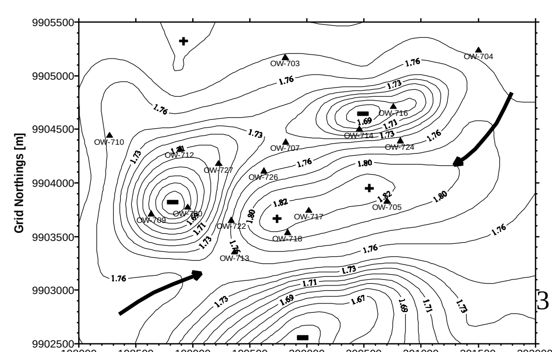

Fig 5. Vp/Vs distribution in the North East Field

The low $\mathbf{V_p/V_s}$ zone starts from OW-716, through OW-707 to OW-727 and OW-709 that have been found to have high temperatures. A NE-SW zone of high value extends southward from OW-704 to OW-705, OW-717, OW-718, and OW-713. This zone might be related to less steam and higher water saturation. This leads to higher water pressure and lower temperatures along this trend. This has lead to faster cooling of the system.

A contoured map of pressure values at 500 masl [Fig. 6] shows low values in the center of the field that decreases southwards towards the EPF. Low-pressure sinks can be seen at wells OW-716, OW-709 and OW-726 coincident with the low $\mathbf{V_p/V_s}$ areas. This is interpreted to represent high temperature deep reservoir fluid up-flow zones.

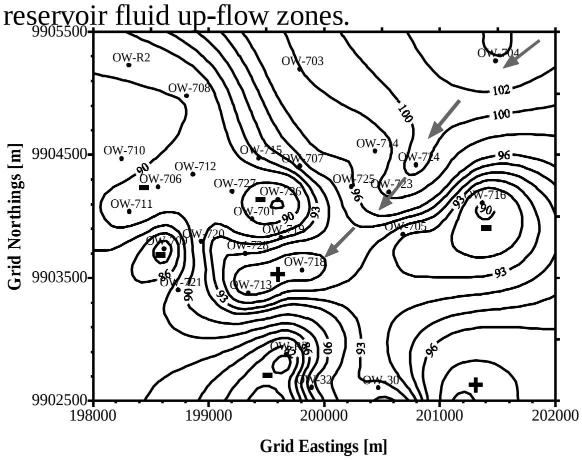

Fig 6. Stable downhole pressure in the NEF

A zone of high pressure extends along a NE-SW trend [shown by arrows] from OW-704 to OW-718 and OW-713. This high-pressure zone has been interpreted to represent the cold recharge for the field from the NE. This result is consistent with $\mathbf{V_p/V_s}$ [Fig. 5] that show the recharge zones are characterized by higher values and the up-flow zones by lower values.

East Production Field [EPF]

On average, $\mathbf{V_p/V_s}$ values in the EPF [Fig. 7] are much lower than those determined in the NEF. This is expected because the EPF has been under exploitation for the last 15 years during which there has been a steady decline in the total mass output. Prolonged steam exploitation has the effect of lowering the reservoir pressure that in turn induces boiling thus expanding the steam zone. To arrest the decline and for environmental purposes [fluid waste disposal], a re-injection/injection program was initiated using both cold and hot fluids in the center of the field (OW-03 and OW-12). This has resulted in an increased total mass output but with a slight reduction in enthalpy.

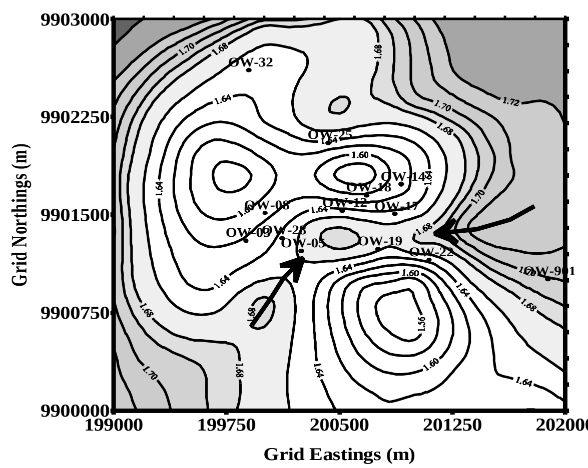

Fig. 7 Vp/Vs distributions in the EPF

Fig. 7 also shows an EW trending zone [with arrows] that has high $\mathbf{V_p/V_s}$ values and divides the EPF field through the center into a northern and southern sector. This implies that there is steam depletion in the center of the field.

An analysis of the reservoir total chloride concentrations within the field for the last ten years was carried out during this study [Fig. 8]. Also reservoir fluid conductivity changes from 1982 [when exploitation started] to 1997 were plotted for two wells [Fig. 9]. One well was chosen from the area that had high $\mathbf{V_p/V_s}$ values [OW-19] and the second well from the area with low values [OW-18].

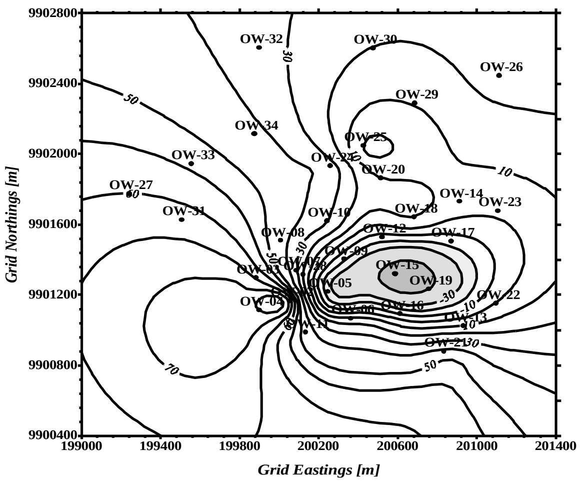

Fig. 8 Contour map of measured % of total chloride changes in the reservoir [1982-1997]

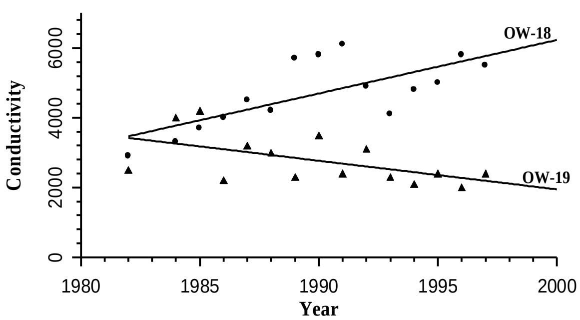

Fig. 9 Reservoir fluid conductivity in well OW-18 and OW-19 from 1982 to 1997

It is seen that most wells in the field coincident with low $\mathbf{V_p/V_s}$ zones show increased chloride concentration and conductivity with time. This increase is expected in view of the continuous exploitation of the field. Wells in the center of the field coincident with the high $\mathbf{V_p/V_s}$ zone show a decrease in the total chloride. The wells in the high $\mathbf{V_p/V_s}$ zone [eg OW-19] showed a decrease in conductivity while the wells in the low $\mathbf{V_p/V_s}$ zone [eg. OW-18] showed an increase in conductivity over the period under exploitation. This implies that there is dilution of the original reservoir waters in the high $\mathbf{V_p/V_s}$ zone. These results are consistent with $\mathbf{V_p/V_s}$ values that are interpreted to show steam depletion/reduction in the center of the field due to the combined effect of cold injection into the system and possible inflow of recharge fluids from the eastern edge.

DISCUSSIONS

This study has shown that the lower $\mathbf{V_p/V_s}$ value in the EPF is related to fluid exploitation for electric power generation. This has lead to pressure drop and boiling that has increased the amount of steam in the reservoir tending towards steam domination. The NEF is mainly water dominated as such increasing the ratio above the EPF level. The low $\mathbf{V_p/V_s}$ and **s** values in the OWF and Domes field imply that although there has been no exploitation, the reservoirs might vapor/gas dominated with possible higher temperature and fracture density than the NEF.

The Olkaria south [OSF] and OCF show the highest values. This implies that this zone has low fracture density, low temperature and possibly no steam zone. An important feature of these ratios is that they are high outside the geothermal prospect area. This implies that they are controlled by temperature, amount of fracturing and liquid/steam concentrations.

This implies that the lower temperature recharge fluids have the effect of reducing the amount of steam within the reservoir by lowering temperature and increasing pressure thus causing condensation.

Conversely, in the productive field [eg. EPF] pressure draw-down leads to boiling and phase separation. The steam formed preferentially travels faster than the water carrying with it all volatile components. This leads to concentration of the water phase with the non-volatile components such as chlorides and will also lead to increased reservoir fluid conductivity.

The high $\mathbf{V_p/V_s}$ zone in the center of the EPF is a result from steam depletion by condensation due to an EW inflow of natural cold recharge fluids and excessive injection in the center of the field

CONCLUSIONS

Magnitude, frequency and depth distribution show that the brittle-ductile transition zone in the study area is at 4-5 km and the main heat source is at a depth of not less than about 6 km.

$\mathbf{V_p/V_s}$ and Poisson's ratios [**s**] vary from 1.55 to 1.87 and 0.16 to 0.28 respectively and being lowest in the EPF and highest in the OCF. The very low ratios in the EPF is due to exploitation induced phase changes. The low values in the OWF and Domes are due to high fracture density, temperature and high steam/water ratio in the reservoir. The higher values in the NEF are due to the system being more water saturated with less steam and high reservoir pressure. The OSF and OCF fields are likely to be water saturated and have lower temperatures. The two fields might also be located along recharge pathways for the whole Olkaria geothermal system system.

An important result of this study is that $\mathbf{V_p/V_s}$ and **s** determination and analysis if carried with other constraints, can be easy and cost effective tools for determining the status of reservoir fluids within a geothermal field. This can be used at the exploration stage to determine the reservoir status before more expensive exploration drilling is undertaken. $\mathbf{V_p/V_s}$ and **s** can be used as tools for determining up-flow and recharge zones of a geothermal system. During long term injection programs in steam dominated systems $\mathbf{V_p/V_s}$ interpretations will give valuable information on the breakthroughs.

ACKNOWLEDGEMENTS

I wish to thank Elvis Oduong, Samuel Mungai and Tom Mboya of the Kenya Electricity Generating Company who worked tirelessly to collect data. The Scientists at the Geothermal project were very helpful with suggestions that improved this manuscript. Special thanks go to the US Department of Energy and the Division of Ocean and Earth Sciences, at Duke University for financial support. The Department of Geological Sciences at the University of Texas [El Paso] provided us with the RefTek seismic instruments.

REFERENCES

Clarke, M.C.G. and Woodhall, D.G., [1987]. Geological and Geothermal Mapping, British Geological Survey, Exploration for Geothermal Energy Project, *Progress reports No, BGSKEN/2. Unpublished report*, pp135.

Ito H., DeVibriss J., and Nur A., [1979]. Compressional and Shear waves in saturated rock during water-steam transition. *J. Geophys. Res*., 84, 4731-4735.

Kohlstedt D. L., Evans B., and Blackwell S. J., [1995]. Strength of the lithosphere: Constraints imposed by laboratory experiments. *J. Geophys. Res.*, 100[B9], 17587-17602.

Lee, W.H.K., and Lahr. J.C., [1975]. HYPO 71 [revised]: a computer program for determining hypocenter, magnitude and first motion pattern of local earthquake. *USGS, Open File Report*, 75-311.

Lee, W.H.K., Bennett, R.E. and Meagher, K.L., [1972] A method for estimating magnitude of local earthquakes from signal duration. *USGS*. Open File Report, 37pp.

Meissner, R and Strehlau, J., [1982]. Limits of stress in the continental crust and their relation to depth-frequency distribution of shallow earthquakes. *Tectonics*, 1, 73-89.

Muchemi, J., [1994]. Geological interpretation of the Olkaria North East field. *KPC Internal Report* 25pp.

Muchemi, J., [1998]. Geological and Structural interpretation of the Greater Olkaria Geothermal field. In: Z.W. Muna [Editor]. Conceptualized model of the Greater Olkaria Geothermal field, *KPC Internal Report. First Edition.*

Z.W. Muna [1998]. Conceptualized model of the Greater Olkaria Geothermal field, *KPC Internal Report. First Edition*.

Mungania, J., [1995]. Tephra deposits in Olkaria and the surrounding areas. *KPC Internal Report*. 7 pp.

Ofwona J., [1998]. Reservoir interference studies in the Olkaria North East field. *KPC Internal Report* 37pp.

Walter A. W., and Weaver C. S., [1980] Seismicity of the Coso Range, California. *J. Geophys. Res.,* 85, 2441-2458.

Wheildon J., Morgan P., Williamson K. H., Evans T. R., and Swanberg C. A., [1994] Heat flow in the Kenya rift zone. In: C Prodehl, G. R. Keller and M. A Khan [Editors]. Crustal and upper mantle structure of the Kenya rift. *Tectonophysics, 236*, 131-149.